Lagrangian temperature, velocity and local heat flux measurement in Rayleigh-Benard convection

Yoann Gasteuil, Woodrow Shew, Mathieu Gibert, Francesca Chillà, Bernard Castaing, Jean-François Pinton

Lagrangian temperature, velocity and local heat flux measurement in Rayleigh-Bénard convection

Y. Gasteuil, W.L. Shew, M.Gibert, F. Chillá, B. Castaing and J.-F. Pinton
Laboratoire de Physique, de l'École Normale Supérieure de Lyon, CNRS UMR5672, 46 Allée d'Italie, 69007 Lyon, France

We have developed a small, neutrally buoyant, wireless temperature sensor. Using a camera for optical tracking, we obtain simultaneous measurements of position and temperature of the sensor as it is carried along by the flow in Rayleigh-Bénard convection, at $Ra \sim 10^{10}$. We report on statistics of temperature, velocity, and heat transport in turbulent thermal convection. The motion of the sensor particle exhibits dynamics close to that of Lagrangian tracers in hydrodynamic turbulence. We also quantify heat transport in plumes, revealing self-similarity and extreme variations from plume to plume.

PACS numbers: 47.80.-v (Instrumentation for fluid flows); 44.27.+g (Convective heat transfer)

Understanding fluid motion and transport of heat due to thermal convection is crucial for progress in diverse challenging and important problems such as climate change, processes in planetary and stellar cores, and efficient temperature control in buildings. Numerous laboratory studies employing Rayleigh-Bénard experiments have uncovered laws which relate global heat flux and flow velocities to fluid properties, flow boundary geometry, and driving parameters [1]. More recently, several studies [2, 3] have focused on coherent flow structures, called plumes, which are ejected from the thermal boundary layers carrying heat into the convective flow. We present measurements from a novel temperature sensor which is carried along with the convective flow, i.e. Lagrangian measurements. In this way we obtain statistics of simultaneous velocity, temperature, and heat transport dynamics throughout the lifetimes of many plumes.

Lagrangian measurements are particularly well suited for studying flows where coherent structures [4] and mixing [5] are important, e.g. plumes mixing temperature in convection. Recent Lagrangian experiments with submillimeter-sized passive tracer particles have advanced understanding of turbulence [6, 7, 8, 9]. In the context of convection, Lagrangian measurements have long been performed using meter-sized atmospheric balloons [10] or ocean floats [11]. Here we use a similar strategy, aided by advances in miniature sensors and communication devices [12], to probe temperature and flow properties at centimeter scales in Rayleigh-Bénard convection.

Our experimental setup is a rectangular vessel with height $H = 40$ cm and section 40 cm $\times$ 10 cm filled with water (for more detail, see [13]). The walls are made of poly-methylmetacrylate (PMMA), the top boundary is a copper plate chilled by a controlled water bath, and the bottom boundary is an electrically heated copper plate. The heater power is maintained at 230 W and the top plate is held at $T_{\rm up} = 19$°C, resulting in a temperature difference $\Delta T = 20.3$°C between the top and bottom plates. The resulting Rayleigh number is $Ra = g\beta\Delta T H^3/\nu\kappa = 3 \times 10^{10}$, where g is acceleration due to gravity, $\beta = 2.95 \times 10^{-4}$ K^{-1} is the thermal expansion coefficient of water and $\nu = 8.17 \times 10^{-7}$m^{2}s^{-1}, $\kappa = 1.48 \times 10^{-7}$m^{2}s^{-1} its viscosity and thermal diffusivity (values are given for the mean temperature of the flow 29.1°C). The Nusselt number, defined as the total heat flux normalized by $\kappa\Delta T/H$, is $Nu = 167.9 \pm 0.2$. Under these conditions, the convective regime is fully turbulent [13, 14, 15] and the mean flow is a steady, system-sized, convection roll with a rotation period of about 100 s.

The mobile sensor consists of a $D = 21$ mm diameter capsule containing temperature instrumentation, an RF emitter, and a battery. It is described in detail in [12] and we recount its basic features here. The capsule and fluid density are carefully matched within 0.05 percent so that it reliably follows the flow. Four thermistors (0.8 mm, 230 kΩ, response time 0.06 s in water) are mounted in the capsule wall protruding 0.5 mm into the surrounding flow. A resistance controlled oscillator is used to create a square wave whose frequency depends on the temperature of the thermistors. This square wave is used directly to modulate the amplitude of the radio wave generated by the RF emitter. The temperature signal is recovered on-the-fly by a stationary receiver and a Labview program. The dynamic range of temperature detection is 80dB, with a resolution of 4 mK and 50 ms. In addition, the capsule trajectory is recorded with a digital video camera, providing synchronous measurements of the position and temperature of the sensor as it is carried about by the fluid. With maximum flow velocities in the range 1-2 cm/s and a particle size of 21 mm, we are oversampling the dynamics by a factor of order 10. However, the characteristic thickness of the thermal boundary layer is $\ell_T \sim \frac{1}{2}HNu^{-1} \sim 1.2$ mm and that of the hydrodynamic boundary layer may be estimated [1] as $\ell_U \sim \ell_T(\nu/\kappa)^{+1/3} \sim 2$ mm. Thus, the sensor is too large to penetrate the boundary layers.

Before presenting more detailed statistics, we provide an overview of the raw data collected by the mobile sen-

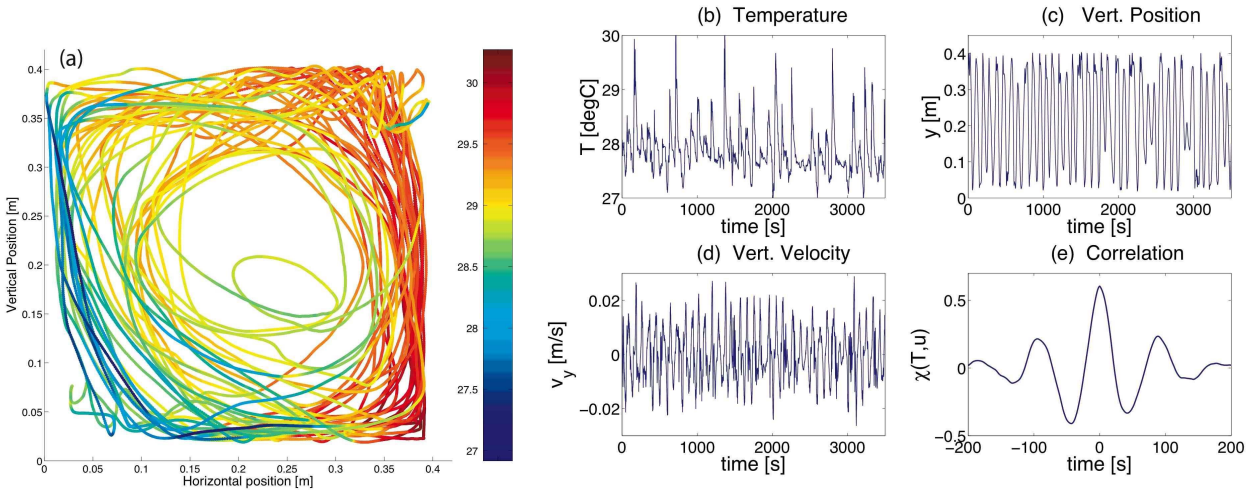

FIG. 1: Temperature and velocity measurements of the mobile sensor. (a) trajectory with temperature color coding; (b) temperature; (c) vertical position; (d) vertical velocity; (e) cross correlation of temperature and velocity.

sor. Predominantly, the sensor moves in looping trajectories the size of the convection cell with a period of about 100 s. The collective result of many fluid parcels (plumes) with such trajectories compose the large scale convection roll – one may also detect in Fig.1a the presence of secondary rolls in the lower left and upper right corners. Although the main motion of the sensor is rather periodic, we point out that its temperature fluctuates widely and irregularly (see Fig.1b, c, d.) Fig.1e shows the cross-correlation between temperature and normalized velocity. We find a maximum value of 0.6 at zero-time lag and confirmation of the 100 s period of the large scale roll. This correlation is about twice the value reported in [17] for local Eulerian measurements. We attribute these dynamics to the entrainment of the sensor by thermal plumes and associate the fluctuations in Figs1.b-d with variation between plumes. In addition to qualitative verification of this idea using Schlieren visualizations, it is consistent with previous studies which find plumes predominately near the side walls like the trajectory of our sensor [16, 17]. We explore these dynamics quantitatively in the results to follow.

From the data in Fig.1, one may estimate characteristic dimensionless numbers for the flow. From integral quantities one computes the integral Reynolds number $Re = UH/\nu \sim 4000$. The associated turbulent – Taylor based – Reynolds number is of the order of $R_\lambda \propto \sqrt{Re} \sim 63$. We note that this value is very close to a local Reynolds number, defined from the actual motion of the Lagrangian sensor $Re' = u_{rms}\ell_{rms}/\nu \sim 60$, where ℓ_{rms} is the fluctuation of position along a 'mean' trajectory, u_{rms} is the usual standard deviation of the velocity. In this regime ($R_\lambda \sim 60$), one expects turbulence with significant intermittency in the velocity gradients [18].

Accordingly, we turn now to more detailed statistics of our measurements including power spectra, increment probability distribution functions (PDF), and structure function scaling for velocity and temperature. The power spectra (in time) are shown in Fig.2a. The velocity spectrum is close to the behavior expected for a Lagrangian tracer in a turbulent flow – f^{-2} – although scaling range is limited at such low R_λ. The temperature spectra is observed to roughly mimic that of velocity with a steeper power law slope compared to measurements with a stationary temperature probe. For such Eulerian measurements, experiments [19] measure slopes between -1.35 and -1.4 ($\equiv -7/5$) while numerical studies [20] report -7/5 in the bulk and -5/3 near the side walls. Velocity increments (Fig.2b) indicate that the sensor is subjected to rather intermittent acceleration with strongly non-Gaussian statistics – flatness is -21. Like the power spectrum, the shape of PDFs for different velocity increments is similar to those of a fluid particle in a turbulent flow – Fig.2b. Finally, we have computed the evolution of the structure functions for the vertical velocity $S^p_{vz}(\tau) = \langle |v_z(t+\tau) - v_z(t)|^p \rangle_t$; we observe an extended region of relative scaling $S^p_{vz}(\tau) \propto [S^2_{vz}(\tau)]^{\xi_p}$ (for 0.3 s $\leq \tau \leq$ 10 s) with exponents $\xi_1 = 0.56, \xi_2 = 1.00, \xi_3 = 1.30, \xi_4 = 1.50, \xi_5 = 1.65, \xi_6 = 1.7$. These values (determined with a 10% precision) are again in good agreement with experimental measurements for Lagrangian tracers in turbulence [7]. We also show in Fig.2c the probability density function (PDF) of temperature increments measured by the mobile sensor. Similar to Eulerian measurements [17], their statistics are non Gaussian, with wider tails at small scale. In contrast to the velocity behavior (and to some Eulerian studies [20]), our Lagrangian temperature increments do not reveal a range of self-similar scaling.

As proposed in several previous studies [16, 21, 22],

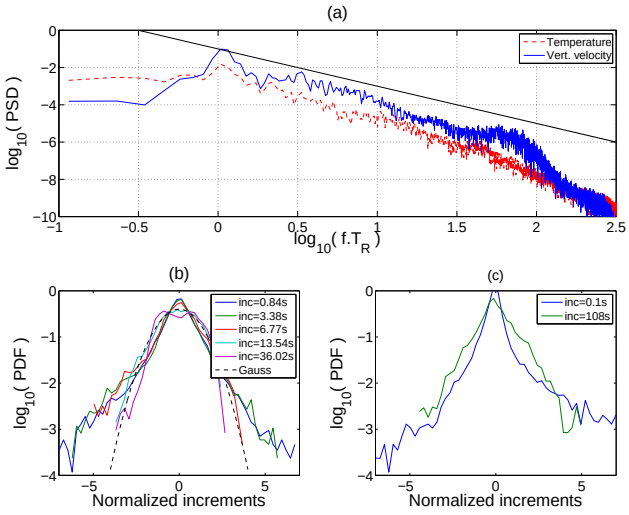

FIG. 2: Temperature and velocity statistics. (a) Time spectra of temperature and vertical velocity of the sensor particle; the frequency is non-dimensionalized using the period $T_R = 100$ s of the large scale roll motion and curves have been shifted vertically for clarity). The solid straight line corresponds to an ideal f^{-2} scaling; (b) PDFs of vertical velocity increments (time lags are given in the inset); (c) PDFs of temperature increments for time lags equal to 0.1 and 102.4 s.

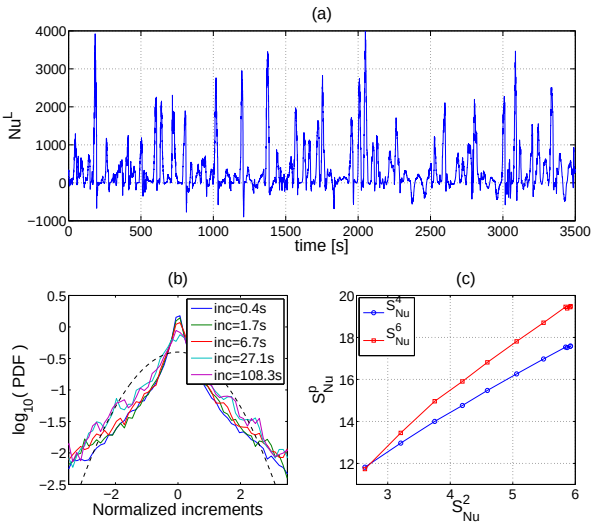

FIG. 3: Lagrangian heat transport. (a) time series; (b) PDF of increments, and Gauss distribution (dashed line). (c) ESS plot of fourth and sixth order structure functions, *vs* the second order one (the second order structure function has been shifted vertically).

the dynamics of heat transport may be best analyzed in terms of a local heat flux $v_z\theta'(t)$, where $\theta'(t) = \theta(t) - \overline{\theta}$ is the particle temperature variation from its time averaged temperature $\overline{\theta}$, and $v_z(t)$ its vertical velocity. Our mobile sensor allows for a Lagrangian measurement of this quantity. In particular, we define a normalized Lagrangian vertical heat transport

$$Nu^L(t) = 1 + \frac{H}{\kappa \Delta T}\, v_z(t)\theta'(t)\ . \qquad (1)$$

The time series $Nu^L(t)$ is shown in Fig.3a. As expected, it is most often positive since convective motions are associated with either hot fluid rising or cold fluid sinking, in each case $(v_z\theta') > 0$. The much less probable events with $(v_z\theta') < 0$ correspond, for instance, to the rise of the particle when it is colder than its environment due to turbulent swirls in the flow. We find that the time averaged Lagrangian heat transport $\overline{Nu^L} = 328$ is larger than the global value ($Nu = 168$ in our case). This indicates that our sensor preferentially samples the regions of the flow which carry higher than average heat, i.e. plumes. In contrast, the traditional Nusselt number indiscriminately accounts for all regions in the flow such as the center of the cell where plumes rarely visit. Another prominent feature is the highly non-Gaussian, intermittent fluctuations of Lagrangian heat transport, which is similar to measurements with stationary probes at similar Rayleigh numbers [17].

To further quantify Lagrangian heat transport, we have studied the statistics of the increments (in time) $Nu^L(t+\tau) - Nu^L(t)$. Two features are noteworthy: (i) as shown in Fig.3b, their PDFs are strongly non Gaussian from the smallest time increments to lags of the order of integral time T_R; (ii) there exists a range of relative scaling for their structure functions $S^p_{Nu}(\tau) = \langle |Nu^L(t+\tau) - Nu^L(t)|^p \rangle_t$, as shown in Fig.3c. The relative exponents, $S^p_{Nu}(\tau) \propto [S^2_{Nu}(\tau)]^{\xi^{Nu}_p}$ have values $\xi^{Nu}_1 = 0.54, \xi^{Nu}_2 = 1.00, \xi^{Nu}_3 = 1.37, \xi^{Nu}_4 = 1.68, \xi^{Nu}_5 = 1.93, \xi^{Nu}_6 = 2.14$ – the use of the second order structure function as a reference is arbitrary. Comparison with the velocity shows that the Lagrangian heat flux is less intermittent; i.e. the PDFs of the local heat flux in Fig.3b are non Gaussian but their shapes do not evolve significantly as increments increase towards the large scale period T_R.

A simple interpretation of the above statistical results is that thermal plumes may be defined as Lagrangian heat transport events (once detached from the thermal boundary layer); these events are in some way self-similar as will become clear below. In this light, we have analyzed the portions of the sensor trajectories during which its vertical position lies between $H/4$ and $3H/4$, i.e. the rise (or fall) of a hot (cold) plume. For each of these motions, we compute the mean heat transport, and its fluctuation measured by the standard deviation computed over the portion of the trajectory. The results are reported in Fig.4. We observe that the heat transport has large variations from one plume to the next. The mean Lagrangian heat transport in these events ($\overline{Nu^{\rm pl}} = 335$) is quite close to the mean for the entire time series ($\overline{Nu^L} = 328$), which indicates that the times the sensor is

not in a plume are relatively unimportant to heat transport. Furthermore, the variation from plume to plume is quite large, $\mathrm{rms}(Nu^{\mathrm{pl}}) = 384$, of the order as the mean. During the trajectory of a single plume, the standard deviation σ of Nu^{pl} is proportional to the mean; $\sigma = \alpha\overline{Nu^{\mathrm{pl}}}$ where $\alpha = 0.5 \pm 0.05$. We note that the plume heat transport we measure matches within a factor of 2 the prediction of the model proposed in [22], though more experiments are required to test scaling laws for different Rayleigh numbers and fluid properties. Furthermore, we find that the characteristic time for temperature decay during the life-time of a plume is of the order of its travel time from one plate to the other, which also supports the model in [22].

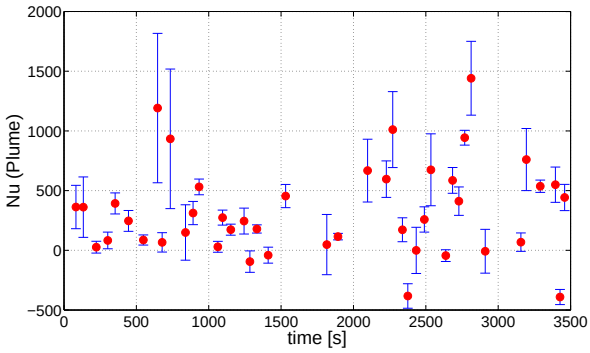

FIG. 4: Plumes. Mean (dots) and standard deviation (error bars) of Lagrangian heat transport of consecutive plumes.

To summarize, we have reported novel measurements of Lagrangian temperature and heat transport using a wireless, neutrally buoyant temperature sensor. The sensor provides a new perspective on the dynamics of thermal plumes in turbulent Rayleigh-Bénard convection. We find that heat transport fluctuates greatly from one plume to another and that these fluctuations suggest a self-similar character of plumes. A practical implication of our results is that in order to maximize heat transport, one should maximize the production of thermal plumes. This is supported by global Nu versus Ra measurements in experiments [23, 24] with rough endplates. Future investigations will be focused on the scaling of plume heat transport for varying Ra and different fluids.

Acknowledgements

This work has been supported by Emergence Rhône-Alpes Contract No. 2005-12 and CNRS. We acknowledge useful discussions with Sergio Ciliberto and Romain Volk.

[1] See S. Grossmann, D. Lohse, *J. Fluid Mech.* **407**, 27 (2000) for a review of scaling possibilities, and references therein of associated experimental measurements.
[2] Q. Zhou, C. Sun, K.-Q. Xia, *Phys. Rev. Lett.* **98**, 074501 (2007)
[3] S. Sun, Q. Zhou, K.-Q. Xia, *Phys. Rev. Lett* **97**, 144504 (2006)
[4] M. A. Green, C. W. Rowley and G. Haller, *J. Fluid Mech.*, **572** 111 (2007)
[5] R. O. Fox, P. K. Yeung, *Phys. Fluids*, **15** 961 (2003)
[6] S. Ott, J. Mann, *J. Fluid Mech.*, **422** 207 (2000)
[7] N. Mordant et al. *Phys. Rev. Lett.*, **87**(21), 214501, (2001); N. Mordant, P. Metz, O. Michel, J.-F. Pinton, *Rev. Sci. Instr.* **76** 025105 (2005)
[8] La Porta A.L., *et al.*, *Nature*, 409, 1017, (2001); H. Xu et al. *Phys. Rev. Lett.* **96**, 024503 (2006); M. Bourgoin et al., *Science* **311**, 835 (2006).
[9] B. Luthi, A. Tsinober, W. Kinzelbach, *J. Fluid Mech. 528*, 87 (2005)
[10] F. Gifford, it Month. Weather Rev. **83**(12), 293 (1955) S. Hanna, *J. Appl. Meteo.* **20**, 242 (1981)
[11] R.-C. Lien, E.A. D'Asaro, G.T. Dairiki, *J. Fluid Mech.* **362**, 177 (1998)
[12] W. Shew et al., *Rev. Sci. Instr.* **78**, 1 (2007)
[13] F Chillá et al., *Nouvo Cimento* **15**, 1229 (1993).
M. Gibert et al. *Phys. Rev. Lett.* **96**, 084501 (2006).
[14] B. Castaing et al., *J. Fluid Mech.* **204**, 1 (1989).
[15] B. Castaing, Phys. Rev. Lett. 65, 3209 (1990).
[16] X.-D. Shang, X.-L. Qiu, P. Tong, K.-Q. Xia, *Phys. Rev. Lett.* **90**(7), 074501 (2003)
[17] X.-D. Shang, X.-L. Qiu, P. Tong, K.-Q. Xia, *Phys. Rev E* **70**, 026308 (2004)
[18] B. W. Zeff, D. D. Lanterman, R. McAllister, R. Roy, E. J. Kostelich, D. P. Lathrop, *Nature* **421**, 146 (2003)
[19] J. A. Glazier, T. Segawa, A. Naert and M. Sano, *Nature* **398**, 307 (1999)
X. Z. Wu, L. Kadanoff, A. Libchaber, and M. Sano, *Phys. Rev. Lett.* **64**, 2140 (1990).
[20] R. Verzicco, R. Camussi, *J. Fluid Mech.* **477**, 19 (2003)
[21] E.S.C. Ching et al. , *Phys. Rev. Lett.* **93**(12), 124501 (2004)
[22] S. Grossmann, D. Lohse, *Phys. Fluids* **16**(12) 4462 (2004)
[23] R. Camussi, R. Verzicco, *Eur. J. Mech. B/Fluids* **23**, 427 (2004)
[24] S. Cilberto, S. Cioni, C. Laroche, *Phys. Rev* **E54**, R5901 (1996)